

Orbital Ordering and Unfrustrated $(\pi, 0)$ Magnetism from Degenerate Double Exchange in the Pnictides

Weicheng Lv, Frank Krüger, and Philip Phillips

Department of Physics, University of Illinois, 1110 West Green Street, Urbana, Illinois 61801, USA

(Dated: December 14, 2019)

We propose a local-itinerant theory to explain the anisotropic electronic and magnetic properties of the iron pnictides. An isotropic, strongly frustrated J_1 - J_2 Heisenberg model describes the local moments. We further introduce a strong Hund's coupling between the local moments and the itinerant bands of the degenerate d_{xz} and d_{yz} orbitals. The system spontaneously develops ferro-orbital order because of the kinetic energy gained by hopping along ferromagnetic spin chains which are stabilized by the double-exchange mechanism. By calculating the spin-wave dispersion in the presence of super- and double-exchange, we find that the emergent ferro-orbital order leads to a dramatic increase of the spin-wave energies at the competing Néel ordering wave vector. The spectra are in good agreement with recent neutron scattering data and suggest a strong anisotropy of the magnetic exchanges on the level of an effective spin-only model. Remarkably, the ferromagnetic double-exchange contribution can exceed the bare super-exchange J_1 leading to an effective ferromagnetic exchange along the y -direction and hence to unfrustrated $(\pi, 0)$ -stripe antiferromagnetism.

PACS numbers: 74.70.Xa, 75.25.Dk, 74.25.Ha, 71.10.Fd

I. INTRODUCTION

The discovery of superconductivity in the pnictides¹⁻⁶ with record transition temperatures challenging those of single-layer, high- T_c cuprates, immediately raised the question of whether, despite all their differences, the two classes of materials share the same key mechanism for superconductivity.⁷⁻⁹ Arguably the most striking similarity is that superconductivity emerges upon doping antiferromagnetically ordered parent compounds. However, in the pnictides, the magnetic ordering is unusual, characterized by an antiferromagnetic arrangement of ferromagnetic chains, corresponding to an in-plane ordering wave vector $\mathbf{Q} = (\pi, 0)$.¹⁰⁻¹⁹ Whereas the pnictides are metallic, the parent cuprates are Mott insulators. The conductivities in the pnictides are typical of bad metals, suggesting that electronic correlations²⁰⁻²⁹ are crucial. By contrast, the local-density approximation (LDA) seems to be adequate³⁰ to describe their band structure.

As a result of this dichotomy, both itinerant magnetism³⁰⁻³⁶ and local moment^{27-29,37-42} scenarios have been suggested to explain the unusual stripe antiferromagnetism. In the former weak-coupling theories, magnetism arises from a spin-density wave instability as a result of a nested Fermi surface. In the latter, local moments arise from correlation effects. In fact, there is increasing evidence that the interaction energies are comparable to the electronic bandwidth²¹⁻²⁶ identifying the systems as moderately coupled. Certainly, the weak-coupling theories provide a simple setting for studying different pairing instabilities. The magnetic excitation spectra however, measured in great detail by inelastic neutron scattering,^{43,44} so far have been rationalized only by using suitable parametrized Heisenberg models.

Because of the positions of the arsenic ions above or below the iron plaquettes, such a spin-only model is expected to be strongly frustrated with comparable,

antiferromagnetic super-exchange couplings J_1 and J_2 between nearest and next-nearest neighbor spins, respectively. In this regime, the model indeed exhibits long-range stripe-antiferromagnetic order⁴⁵⁻⁴⁷, and the strong frustration and proximity to a continuous magnetic phase transition might explain why the observed magnetic moments are relatively small.^{27,40} However, the neutron scattering experiments tell a radically different story. The measured spin-wave velocities indicate a strong anisotropy between the nearest-neighbor super-exchange couplings along the two in-plane lattice directions⁴³, $J_{1x} \gg J_{1y}$. More recent data covering the entire spectrum⁴⁴ suggest that the weaker coupling is even slightly ferromagnetic corresponding to an unfrustrated spin model in contrast to early claims²⁷ of high frustration.

What might be the cause of such a strong spatial anisotropy? In fact, before the magnetic order sets in, a structural transition occurs at which the two in-plane lattice constants become inequivalent. The structural and magnetic transition are clearly separated in the so-called '1111 compounds',¹⁰⁻¹³ whereas they occur at the same temperature in the '122 family'.¹⁴⁻¹⁷ However, inspecting the numbers, it appears that the orthorhombic lattice distortion is too small, by two orders of magnitude, to explain the magnetic anisotropy.⁴²

To this end, some have proposed^{38,48,49} that orbital-ordering physics of a similar kind as in the manganese transition-metal oxides not only provides a mechanism for the lattice distortion but more importantly explains the strong in-plane anisotropies. In particular, it has been argued³⁸ that due to an orbital degeneracy, the localized limit is described by a complicated spin-orbital super-exchange (Kugel-Khomskii) model rather than by a Heisenberg Hamiltonian. Further, it was shown that the stripe antiferromagnetism is stabilized by ferro-orbital order which breaks the in-plane lattice symmetry

and induces a strong anisotropy between the magnetic exchange couplings.

Since the C_4 symmetry is broken by the orbital order and the accompanying orthorhombic distortion, the electronic structure must reflect this spatial anisotropy with reduced symmetry.⁵⁰ Such an anisotropic electronic state has been confirmed recently in scanning-tunneling-microscopy (STM) experiments.⁵¹ Moreover, dramatic Fermi-surface reconstructions at the structural transition,⁵² as well as enormous transport⁵³ and phonon⁵⁴ anomalies, have been interpreted as clear indirect evidence for orbital ordering. Hence, on this interpretation, it is the orbital ordering that underlies the electronic anisotropy not an inherent anisotropy due entirely to the electrons, indicative of a true nematic state.

Consequently, an open problem with the pnictides is the role itineracy and local physics play in mediating the apparently unfrustrated anisotropic magnetism. In this work, we start from the idea of the ‘local-itinerant dichotomy’^{20,55,56} of the iron pnictides and motivate an effective degenerate double-exchange model very similar to the ones used to describe metallic manganites with orbital degeneracies.^{57–59} To be more precise, we assume a strong ferromagnetic Hund’s coupling between the local moments, which are described by the aforementioned J_1 - J_2 Heisenberg model, and the itinerant bands of the doubly-degenerate d_{xz} and d_{yz} orbitals. We demonstrate that up to a certain carrier density, the model develops a perfect orbital polarization giving rise to an anisotropic electronic structure. The emergent ferro-orbital order stabilizes the $(\pi, 0)$ antiferromagnetism by directing the kinetic energy along the ferromagnetic spin direction. The calculated magnetic excitation spectra in the presence of both, super- and double-exchange are found to be in good agreement with the neutron scattering data.⁴⁴ By fitting to a \tilde{J}_{1x} - \tilde{J}_{1y} - \tilde{J}_2 spin-only model, we find a strong anisotropy of the effective exchange constants, including a ferromagnetic \tilde{J}_{1y} within some parameter space, as suggested by experiments.⁴⁴ In short, the interplay between the local moments and the itinerant electrons gives rise to orbital ordering, the formation of an anisotropic electronic state, and the magnetic exchange anisotropy, all of which agree with current experimental observations.

This paper is organized as follows. In Sec. II, we construct the local-itinerant, degenerate double-exchange model. Sec. III deals with the methods we use to solve the model. Namely, a canonical transformation is performed to identify the true magnons of the system. In Sec. IV, we summarize our results, including ferro-orbital ordering, the magnetic excitation spectra, and the magnetic anisotropy. Finally Sec. V discusses several aspects of our theory and validates its applicability to the pnictides.

II. MODEL

In this Section, we proceed to motivate the degenerate double-exchange model. This model accounts for the presence of local moments, as suggested by the neutron scattering experiments, as well as itinerant electrons responsible for the bad-metal behavior of the parent compounds. Moreover, the orbital degeneracy in combination with a strong Hund’s coupling between electronic and spin degrees of freedom gives rise to orbital-ordering physics beyond simple band-structure theory. The Hamiltonian consists of three parts,

$$\mathcal{H} = \mathcal{H}_{\text{loc}} + \mathcal{H}_{\text{it}} + \mathcal{H}_{\text{H}}, \quad (1)$$

where \mathcal{H}_{loc} describes the super-exchange couplings between local moments, \mathcal{H}_{it} the itinerant electrons of the degenerate d_{xz} and d_{yz} orbitals, and \mathcal{H}_{H} the ferromagnetic Hund’s coupling between the local moments and the itinerant electrons. In order for this model to be valid, the Hund’s coupling should be small compared to the tetrahedral crystal field splitting between the t_{2g} and e_g multiplets, but larger than the tetragonal splitting between the d_{xy} orbital and the degenerate d_{xz}, d_{yz} doublet.³⁸

The local moments with spin S are coupled by super-exchanges J_1 and J_2 between nearest and next-nearest neighbors, respectively. The corresponding Heisenberg Hamiltonian reads

$$\mathcal{H}_{\text{loc}} = \frac{J_1}{S^2} \sum_{\langle i,j \rangle} \mathbf{S}_i \cdot \mathbf{S}_j + \frac{J_2}{S^2} \sum_{\langle\langle i,j \rangle\rangle} \mathbf{S}_i \cdot \mathbf{S}_j, \quad (2)$$

where, for convenience, the super-exchanges are measured in units of S^2 . Likewise, the Hund’s exchange J_{H} which couples the electron spins to the local moments will be measured in units of S . This convention will facilitate our large- S expansion later. We focus on the regime $J_2 > J_1/2$ where the $(\pi, 0)$ stripe antiferromagnet is one of the classical ground states. For sufficiently large J_2 , quantum fluctuation will stabilize the $(\pi, 0)$ state over other canted, classically degenerate states due to the order-from-disorder mechanism.^{46,47}

In the pnictides, the super-exchange is mediated by virtual hopping processes via the p -orbitals of the arsenic ions which have alternating positions above or below the iron plaquettes. Certainly, a quantitative comparison of the exchange couplings would require knowledge about the precise shape of the orbitals and of the two different Fe-As-Fe bond angles which depend on the distance of the arsenic ions to the iron layers. However, assuming that the virtual processes for the nearest-neighbor and diagonal bonds involve roughly the same energies, we estimate $J_1 \approx 2J_2$ since two exchange paths via different arsenic ions contribute to the nearest-neighbor super-exchange J_1 . Therefore, one should expect the Heisenberg model (2) to be strongly frustrated and potentially in the quantum disordered regime.

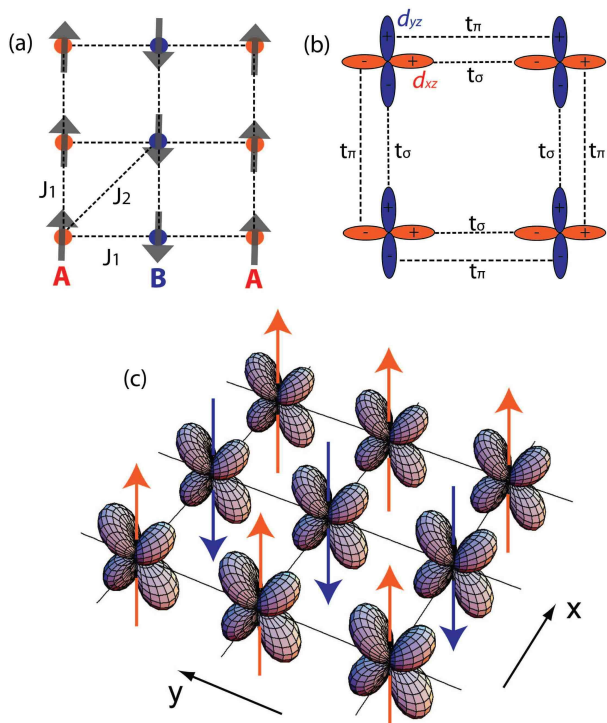


FIG. 1: (Color online) Illustration of the degenerate double-exchange model for the pnictides. (a) The local moments are coupled by nearest- and next-nearest-neighbor exchanges J_1 and J_2 , respectively. We focus on the regime $J_2/J_1 > 1/2$ where the $(\pi, 0)$ stripe antiferromagnetism is classically stable but where the spins might be quantum disordered. The local moments are coupled via a strong ferromagnetic Hund's exchange J_H to the itinerant electrons of the degenerate d_{xz} , d_{yz} orbitals. (b) Illustration of the hopping parameters in a two-band model of these orbitals (shown as projections in the plane). We assume $t_\sigma > t_\pi$ and neglect the hoppings along the diagonal bonds for simplicity. (c) Resulting ferro-orbital order which stabilizes the $(\pi, 0)$ antiferromagnetism by directing the kinetic energy of the electrons along the ferromagnetic spin direction.

The Hamiltonian for the itinerant electrons of the degenerate d_{xz} and d_{yz} orbitals is given by

$$\mathcal{H}_{\text{it}} = - \sum_{ij, \alpha\beta, \nu} t_{ij}^{\alpha\beta} c_{i\alpha\nu}^\dagger c_{j\beta\nu} + \frac{V}{2} \sum_{i, \alpha \neq \beta, \nu\nu'} \hat{n}_{i\alpha\nu} \hat{n}_{i\beta\nu'}, \quad (3)$$

where $c_{i\alpha\nu}^\dagger$ creates an electron at site i on orbital α with spin ν and $\hat{n}_{i\alpha\nu} = c_{i\alpha\nu}^\dagger c_{i\alpha\nu}$. The hopping integrals between neighboring sites are shown in Fig. 1(b) and defined as $t_x^{xz, xz} = t_y^{yz, yz} =: t_\sigma$ and $t_x^{yz, yz} = t_y^{xz, xz} =: t_\pi$. The overlap of different orbitals on neighboring sites is strictly zero, $t_x^{xz, yz} = t_y^{xz, yz} = 0$. We will assume $t_\sigma > t_\pi$ because we expect a larger wave-function overlap when the orbitals point towards one another. However, the precise shape of the orbitals is not determined by geom-

etry but depends on quantum chemistry, for example, on the amount of hybridization between the Fe d -orbitals with the As p -orbitals.²⁰ Here we simply denote the orbitals by d_{xz} and d_{yz} because of the spatial symmetry shared with the atomic Fe orbitals. Recently, it has been suggested⁴⁹ that the hybridization leads to a strong deformation of the orbitals which make the π overlap the dominant one. We point out that for $t_\sigma < t_\pi$ our results persist, the only difference being that the orbital polarization will be inverted in order to maximize the overlap along the ferromagnetic spin direction.

To further articulate the model, we neglect the next-nearest-neighbor orbital-diagonal and orbital-off-diagonal hoppings which have been introduced in previous two-orbital models^{32,60} in order to fit the measured Fermi surfaces on the level of a tight-binding approximation. Such parameters are inherently arbitrary, since the hopping amplitudes are not uniquely determined by a particular constant energy cut⁶⁰ and because the Coulomb interactions and the Hund's exchange are of the order of the electronic bandwidth.^{21–26}

In addition to the electron hopping between orbitals on neighboring sites, we include an on-site Coulomb repulsion V between electrons in different orbitals which leads to an enhancement of the orbital polarization at higher electron densities. To keep our model as simple as possible, we neglect the intra-orbital Coulomb repulsion, the spin coupling between the itinerant bands, and the pair hopping terms.⁶¹ The inclusion of these additional electron-electron interactions would increase the number of parameters in the model and complicate the mean-field decoupling scheme enormously.

Finally the local moments and the itinerant electrons interact by a ferromagnetic Hund's coupling,

$$\mathcal{H}_H = - \frac{J_H}{2S} \sum_{i, \alpha, \nu\nu'} \mathbf{S}_i \cdot c_{i\alpha\nu}^\dagger \boldsymbol{\sigma}_{\nu\nu'} c_{i\alpha\nu}, \quad (4)$$

where $\boldsymbol{\sigma}_{\nu\nu'} = (\sigma^x, \sigma^y, \sigma^z)_{\nu\nu'}$ with σ^α are the standard Pauli matrices and $J_H > 0$. As mentioned before, the Hund's exchange is measured in units of the local moment S . Similar models have been proposed in the context of the pnictides.^{55,56} However, the orbital degeneracy which is the pre-requisite for orbital-ordering physics was not been included.

III. METHOD

In this Section, we outline the approximations and transformation we employ to analyze the complicated degenerate double-exchange model for the pnictides. In similar models for the maganites the problem is typically simplified by treating the local moments as classical spins and assuming an infinitely strong Hund's exchange.^{57–59} In the pnictides, these approximations are not justified since the Hund's coupling is of the order of the electronic bandwidth and since the local moments are small

and presumably best described by the extreme quantum limit, $S = 1/2$. Moreover, we are interested in calculating the magnetic excitation spectra in the presence of super- and double-exchange which will require the inclusion of quantum fluctuations of the spins. Although the spins are small and the Heisenberg model \mathcal{H}_{loc} is strongly frustrated, we argue that it is reasonable to treat the local moments on the level of linear spin-wave theory since the double exchange leads to a dramatic stabilization of the magnetic order. Moreover, it has been argued that the $1/S$ expansion is much better behaved for the $(\pi, 0)$ magnet than for conventional Néel antiferromagnetic order.⁴⁰

Since the Hund's coupling \mathcal{H}_{H} does not conserve the magnons describing the spin-wave excitation of the isolated local moments, we perform a canonical transformation in order to identify the true magnons of the coupled system. Interactions between the itinerant electrons are treated in a self-consistent Hartree-Fock approximation. Readers not interested in the details of this calculation can skip immediately to the results, Sec. IV.

A. Operator rotations

Following the standard treatment of the antiferromagnetic Heisenberg model, we perform the spin rotation $S_i^x = \tilde{S}_i^x$, $S_i^y = \kappa_i \tilde{S}_i^y$, and $S_i^z = \kappa_i \tilde{S}_i^z$ where $\kappa_i = \exp(i\mathbf{Q} \cdot \mathbf{r}_i) = \pm 1$ for sublattice A and B respectively [see Fig. 1(a)]. Representing the rotated spin operators $\tilde{\mathbf{S}}_i$ by Holstein-Primakoff (HP) bosons a_i, a_i^\dagger , to the leading order, $\tilde{S}_i^z = S - a_i^\dagger a_i$, $\tilde{S}_i^+ = \sqrt{2S} a_i$, and $\tilde{S}_i^- = a_i^\dagger \sqrt{2S}$ ($\tilde{S}_i^\pm = \tilde{S}_i^x \pm i\tilde{S}_i^y$), we immediately derive the following expression for \mathcal{H}_{loc} in the linear spin-wave approximation,

$$\mathcal{H}_{\text{loc}}^{\text{sw}} = \sum_q \left[A_0(q) \left(a_q^\dagger a_q + a_{-q}^\dagger a_{-q} \right) + B_0(q) \left(a_q^\dagger a_{-q}^\dagger + a_{-q} a_q \right) \right], \quad (5)$$

where $A_0(q) = (J_1 \cos q_y + 2J_2)/S$ and $B_0(q) = (J_1 \cos q_x + 2J_2 \cos q_x \cos q_y)/S$. In order to leave the Hund's coupling term \mathcal{H}_{H} invariant, we perform exactly the same rotation of the electron spins $\mathbf{s}_{i\alpha} = \frac{1}{2} \sum_{\nu\nu'} c_{i\alpha\nu}^\dagger \boldsymbol{\sigma}_{\nu\nu'} c_{i\alpha\nu'}$. This is achieved by transforming the fermion operators as $c_{i\alpha\nu} = \tilde{c}_{i\alpha\nu}$ for sites i on sublattice A and $c_{i\alpha\nu} = \tilde{c}_{i\alpha\bar{\nu}}$ on sublattice B. In the latter expression, we have defined $\bar{\nu} = \downarrow$ for $\nu = \uparrow$ and vice versa. In terms of the HP boson creation and annihilation operators a_i, a_i^\dagger and rotated fermi operators $\tilde{c}_{i\alpha\nu}, \tilde{c}_{i\alpha\nu}^\dagger$ the Hund's exchange can be written as

$$\mathcal{H}_{\text{H}} = \mathcal{H}_{\text{H}}^{(0)} + \mathcal{H}_{\text{H}}^{(1)} + \mathcal{H}_{\text{H}}^{(2)}, \quad (6)$$

$$\mathcal{H}_{\text{H}}^{(0)} = -\frac{J_{\text{H}}}{2} \sum_{k,\alpha,\nu} \nu \tilde{c}_{k\alpha\nu}^\dagger \tilde{c}_{k\alpha\nu}, \quad (7)$$

$$\mathcal{H}_{\text{H}}^{(1)} = -\frac{J_{\text{H}}}{\sqrt{2S}} \sum_{kq,\alpha} \left(a_q \tilde{c}_{k+q,\alpha\downarrow}^\dagger \tilde{c}_{k\alpha\uparrow} + \text{h.c.} \right), \quad (8)$$

$$\mathcal{H}_{\text{H}}^{(2)} = \frac{J_{\text{H}}}{2S} \sum_{k,qq',\alpha\nu} \nu a_q^\dagger a_{q'} \tilde{c}_{k-q,\alpha\nu}^\dagger \tilde{c}_{k-q',\alpha\nu}, \quad (9)$$

where $\nu = \pm 1$ for up and down spins respectively. $\mathcal{H}_{\text{H}}^{(0)}$ only involves the electronic operators and represents the zeroth-order corrections to the electron energies by the classical background stripe antiferromagnetism. $\mathcal{H}_{\text{H}}^{(1)}$ and $\mathcal{H}_{\text{H}}^{(2)}$ are the couplings between the electrons and the HP bosons, linear and quadratic in the boson operators.

In the following, we include the term $\mathcal{H}_{\text{H}}^{(0)}$ in the itinerant electron Hamiltonian and perform a standard mean-field decoupling of the inter-orbital Coulomb repulsion, yielding the effective free-electron Hamiltonian

$$\begin{aligned} \mathcal{H}_{\text{e}} &= \mathcal{H}_{\text{it}}^{\text{mf}} + \mathcal{H}_{\text{H}}^{(0)} \\ &= \sum_{k,\alpha,\nu} \left[\left(\varepsilon_1^\alpha(k) - \nu \frac{J_{\text{H}}}{2} + V\rho_{\bar{\alpha}} \right) \tilde{c}_{k\alpha\nu}^\dagger \tilde{c}_{k\alpha\nu} \right. \\ &\quad \left. + \varepsilon_2^\alpha(k) \tilde{c}_{k\alpha\nu}^\dagger \tilde{c}_{k\alpha\bar{\nu}} \right], \end{aligned} \quad (10)$$

where $\bar{\alpha} = yz$ for $\alpha = xz$ and vice versa, and $\rho_{\alpha\nu} = \langle \tilde{n}_{i\alpha\nu} \rangle = \langle \tilde{c}_{i\alpha\nu}^\dagger \tilde{c}_{i\alpha\nu} \rangle$ the mean-field densities which we assume to be homogeneous in space and which have to be calculated self consistently. For brevity, we defined $\rho_\alpha = \sum_\nu \rho_{\alpha\nu}$ which is the total density per site in orbital α . Further we have defined $\varepsilon_1^{xz}(k) = -2t_\pi \cos k_y$, $\varepsilon_1^{yz}(k) = -2t_\sigma \cos k_y$, $\varepsilon_2^{xz}(k) = -2t_\sigma \cos k_x$, and $\varepsilon_2^{yz}(k) = -2t_\pi \cos k_x$.

B. Canonical transformation

Apparently, the interaction term $\mathcal{H}_{\text{H}}^{(1)}$ is linear in the HP boson a_i , which shows that these bosons do not represent the Goldstone modes of the system, namely the transverse fluctuations of the total staggered magnetic moments, which consist of not only the local moments, but also the spins of the itinerant electrons. In order to correctly identify the true magnons and carry out the subsequent spin-wave calculations, we need to perform a canonical transformation of the original Hamiltonian $\mathcal{H} = \mathcal{H}_{\text{loc}}^{\text{sw}} + \mathcal{H}_{\text{e}} + \mathcal{H}_{\text{H}}^{(1)} + \mathcal{H}_{\text{H}}^{(2)}$,

$$\begin{aligned} \mathcal{H}' &= e^\Delta \mathcal{H} e^{-\Delta} \\ &= \mathcal{H} + [\Delta, \mathcal{H}] + \frac{1}{2} [\Delta, [\Delta, \mathcal{H}]] + \dots \end{aligned} \quad (11)$$

with Δ a suitable anti-Hermitian operator, $\Delta^\dagger = -\Delta$, such that in the transformed \mathcal{H}' , the terms linear in a_i 's are eliminated. Similar canonical transformations^{62,63} and equivalent perturbative methods⁶⁴ have been used in order to explain ferromagnetism in double-exchange models with a single itinerant band. Up to the leading order, the transformation is determined by

$$[\Delta, \mathcal{H}_e] + \mathcal{H}_H^{(1)} = 0. \quad (12)$$

To find the Δ satisfying Eq. (12), we need to diagonalize \mathcal{H}_e . This unitary transformation $\tilde{c}_{k\alpha\nu} = \sum_n U_{\alpha\nu}^n(k) d_{nk}$ ($n = 1, \dots, 4$ corresponding to the total of 4 electronic bands with 2 orbital and 2 spin degrees of freedom) is easily found numerically where the self-consistency conditions $\rho_{\alpha\nu} = \langle \tilde{n}_{i\alpha\nu} \rangle$ are solved by iteration. In the new fermion basis d_{nk} , the electronic Hamiltonian \mathcal{H}_e is diagonal yielding the electronic bands $E_n(k)$. Moreover, in this new basis, it is easy to verify that Eq. (12) is solved by

$$\Delta = \frac{J_H}{\sqrt{2S}} \sum_{kq, mn, \alpha} \left(\frac{a_q d_{m, k+q}^\dagger d_{nk}}{E_n(k) - E_m(k+q)} \times U_{\alpha\downarrow}^{m*}(k+q) U_{\alpha\uparrow}^n(k) - \text{h.c.} \right). \quad (13)$$

After the canonical transformation (11), the Hamiltonian up to order $1/S$ reads $\mathcal{H}' = \mathcal{H}_e + \mathcal{H}_{\text{loc}}^{\text{sw}} + \mathcal{H}_H^{(2)} + \mathcal{H}'_2$, where $\mathcal{H}'_2 = [\Delta, \mathcal{H}_H^{(1)}] + \frac{1}{2}[\Delta, [\Delta, \mathcal{H}_e]] = \frac{1}{2}[\Delta, \mathcal{H}_H^{(1)}]$. The commutators $[\Delta, \mathcal{H}_{\text{loc}}^{\text{sw}}]$ and $[\Delta, \mathcal{H}_K^{(2)}]$ are of higher orders in $1/S$ and the boson operators, and thus can be dropped in the linear spin-wave approximation. The contributions $\mathcal{H}_H^{(2)}$ and \mathcal{H}'_2 are bilinear in both the bosonic and fermionic operators. After taking the expectation values of the electronic operators with respect to the diagonal electronic Hamiltonian \mathcal{H}_e , we obtain the final spin-wave Hamiltonian

$$\begin{aligned} \mathcal{H}^{\text{sw}} &= \mathcal{H}_{\text{loc}}^{\text{sw}} + \left\langle \mathcal{H}_H^{(2)} + \frac{1}{2}[\Delta, \mathcal{H}_H^{(1)}] \right\rangle_e \\ &= \sum_q \left[A(q) \left(a_q^\dagger a_q + a_{-q} a_{-q}^\dagger \right) \right. \\ &\quad \left. + B(q) \left(a_q^\dagger a_{-q}^\dagger + a_{-q} a_q \right) \right] \end{aligned} \quad (14)$$

with $A(q) = A_0(q) + A_1 + A_2(q)$ and $B(q) = B_0(q) + B_2(q)$. The constant ‘self-energy’ correction, A_1 , arises from $\mathcal{H}_K^{(2)}$ whereas $H'_2 = \frac{1}{2}[\Delta, \mathcal{H}_H^{(1)}]$ generates momentum-dependent corrections to both the ‘self-energy’ and the ‘anomalous amplitude’, which are denoted as $A_2(q)$ and $B_2(q)$. These corrections are expressed as

$$A_1 = \frac{J_H}{2S} \sum_{k,n} f_n(k) \sum_{\alpha,\nu} \nu |U_{\alpha\nu}^n(k)|^2, \quad (15)$$

$$A_2(q) = \frac{J_H^2}{2S} \sum_{k, mn} \frac{f_n(k) - f_m(k+q)}{E_n(k) - E_m(k+q)} \quad (16)$$

$$\times \left| \sum_{\alpha} U_{\alpha\downarrow}^{m*}(k+q) U_{\alpha\uparrow}^n(k) \right|^2,$$

$$B_2(q) = \frac{J_H^2}{2S} \sum_{k, mn} \frac{f_n(k) - f_m(k+q)}{E_n(k) - E_m(k+q)} \quad (17)$$

$$\times \sum_{\alpha\beta} U_{\alpha\downarrow}^{m*}(k+q) U_{\alpha\uparrow}^n(k) U_{\beta\downarrow}^{m*}(k) U_{\beta\uparrow}^n(k+q),$$

where $f_n(k) = 1/(1 + e^{\beta(E_n(k) - \mu)})$ is the Fermi distribution function with μ the chemical potential. The Hamiltonian (14) is diagonalized by a Bogoliubov transformation yielding the spin-wave dispersion

$$\omega(q) = \sqrt{A^2(q) - B^2(q)} \quad (18)$$

of the system in the presence of both super- and double-exchange.

IV. RESULTS

A. Orbital and spin polarization

We start with the inspection of the electronic Hamiltonian \mathcal{H}_e (10) which includes the Hund’s coupling to the local moments on a classical level given by $\mathcal{H}_H^{(0)}$. We focus on the regime $J_2/J_1 > 1/2$ where the $(\pi, 0)$ stripe antiferromagnetism is classically stable. However, strong magnetic frustration might lead to a paramagnetic, quantum disordered state. We point out that even in the regime $J_2/J_1 < 1/2$ where the (π, π) Néel order is favored on the classical level, the Hund’s exchange will eventually induce a stripe antiferromagnetic spin background once the kinetic energy gains by hopping along ferromagnetic spin directions win out against the difference of magnetic energies of the two spin configurations.

From the self-consistent diagonalization of \mathcal{H}_e (10) for a given total electron filling n , we obtain the mean-field densities $\rho_{\alpha\nu}$ with $\alpha = xz, yz$ the orbital and $\nu = \uparrow, \downarrow$ the spin index. Obviously, these densities sum up to the total filling of the bands, $n = \sum_{\alpha\nu} \rho_{\alpha\nu}$. In Fig. 2, the orbital and spin polarizations, $n_o = \sum_{\nu} (\rho_{yz,\nu} - \rho_{xz,\nu})$ and $n_s = \sum_{\alpha} (\rho_{\alpha,\uparrow} - \rho_{\alpha,\downarrow})$ are shown as a function of the total filling n for different values of the Hund’s coupling J_H/t_σ , the hopping anisotropy t_π/t_σ , and the inter-orbital Coulomb repulsion V/t_σ . Here and in the following all energies are expressed in units of t_σ which is the larger of the two hopping amplitudes. Without the presence of the itinerant electrons, the local moments form

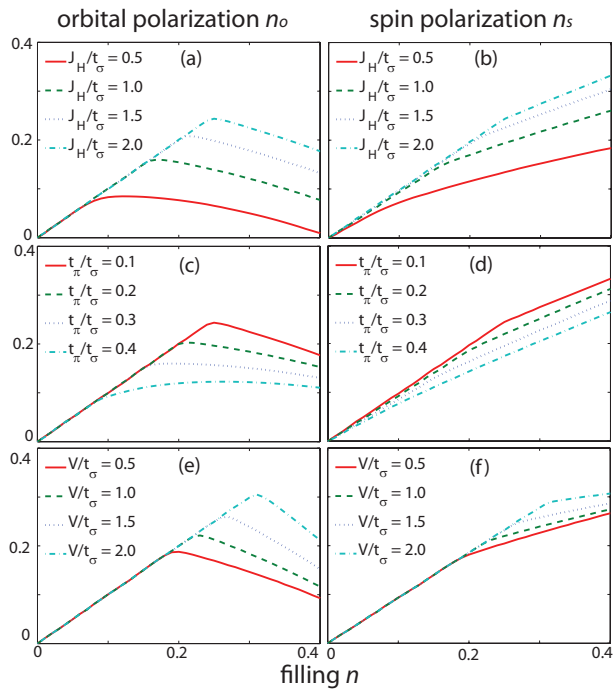


FIG. 2: (Color online) (a, c, e) orbital polarization n_o and (b, d, f) spin polarization n_s as functions of the filling n of the itinerant bands. The other parameters used in each graph are as follows, (a, b) $t_\pi = 0.1t_\sigma$, $V = 0$; (c, d) $J_H = 2t_\sigma$, $V = 0$; (e, f) $J_H = 1t_\sigma$, $t_\pi = 0.1t_\sigma$.

a $(\pi, 0)$ stripe antiferromagnetic ground state. The spins are parallel along the y -direction and anti-parallel along the x -direction, as illustrated by Fig. 1(a). Due to the on-site ferromagnetic Hund's coupling, the spins of itinerant electrons are more likely to be aligned in the same direction as are the local moments on every site. Hoppings along the x -direction put the electrons in the opposite spin states of the local moments either before or after the hopping process, and thus cost more energy in comparison to that involving hopping along the y -direction. With the assumption that $t_\sigma > t_\pi$, the electrons will first occupy the d_{yz} orbitals because of the kinetic energies gained by hopping along the ferromagnetic y -direction. Therefore, the system will form a ferro-orbital-ordered state with all the electrons occupying the d_{yz} orbitals [see Fig. 1(c)] until the Fermi energy reaches the bottom of the band of the d_{xz} orbitals.

This behavior is shown in Fig. 2(a), (c) and (e) for different Hund's coupling J_H , hopping anisotropy and Coulomb repulsion V , respectively. In general, either a larger J_H , or a stronger hopping anisotropy (a smaller t_π), increases the energy difference between the two bands, whereas a greater V also favors orbital polarization to minimize the Coulomb repulsion between the two bands. Hence, all three increase the complete orbital polarization to a higher filling level, as shown by the left column of Fig. 2. We denote the maximum filling level to which the perfect ferro-orbital order is sustained by \bar{n} .

When $n > \bar{n}$, electrons start to populate the d_{xz} orbitals, resulting in a decrease of the orbital polarization n_o .

Furthermore, as being discussed above, the Hund's coupling tends to align the spins of the itinerant electrons with the local moments. Therefore, the electrons are favored in a spin-up state on sublattice A, whereas a spin-down state obtains on sublattice B, corresponding to a spin-up polarized state on both sublattices in the space of the rotated electron operators $\tilde{c}_{i\alpha\nu}$. However, since t_π is non-zero, the expectation values of the spin off-diagonal elements in \mathcal{H}_e (10) are always finite, leading to incomplete spin polarizations, as shown in Fig. 2(b), (d) and (f). Here we have used the same parameters as those used to compute the orbital polarization graphs on the left panel. Generally speaking, a larger J_H or a stronger anisotropy reduces the off-diagonal elements and produces a stronger spin polarization, whereas a greater V does not. However, by increasing V , the maximum spin polarization achieved also increases, although the curve remains unchanged at low fillings. In actuality, assuming $t_\sigma > t_\pi$, we expect that the spin polarization of the d_{yz} orbitals is larger than that of the d_{xz} orbitals. This is indeed reflected by the change in the slope of the spin polarization curves coinciding with the kink in the orbital polarization.

B. Spin-wave spectrum

Now we set out to calculate the spin-wave spectrum by considering the corrections from the itinerant bands to the original, strongly frustrated J_1 - J_2 Heisenberg model. When $n < \bar{n}$, all the electrons occupy the d_{yz} orbitals, leading to enhanced transport along the y -direction. From the knowledge of the double-exchange model, hopping of the itinerant electrons produces an effective ferromagnetic spin exchange between the local moments of neighboring sites. Such induced interactions are stronger along the y - than along the x -direction. Therefore, we expect a strong anisotropy between the effective magnetic exchange couplings which should reduce the magnetic frustration and stabilize $(\pi, 0)$ stripe antiferromagnetism. However, for $n > \bar{n}$, electrons start to populate the d_{xz} orbitals, reducing the orbital polarization. Consequently, in this regime, we expect the magnetic frustration to increase again with the filling n .

Our results for the spin-wave spectra for different filling levels n are shown in Fig. 3(a) for $J_H/t_\sigma = 1.0$, $t_\pi/t_\sigma = 0.1$, and $V = 0$. In this case, the complete orbital polarization is found up to $\bar{n} = 0.16$ [see Fig. 2(a)]. The spin length S of the local moment is $1/2$, which reflects the relatively small moment measured by the experiment¹⁰ and is consistent with a local multiplet structure with an orbital degeneracy.³⁸ We choose $J_1 = 0.04t_\sigma$ so that the exchange constants are of the order of 10 meV for a bandwidth of 1 eV, in agreement with both numerical³⁷ and experimental⁴⁴ observations. Finally the original Heisenberg model is strongly frus-

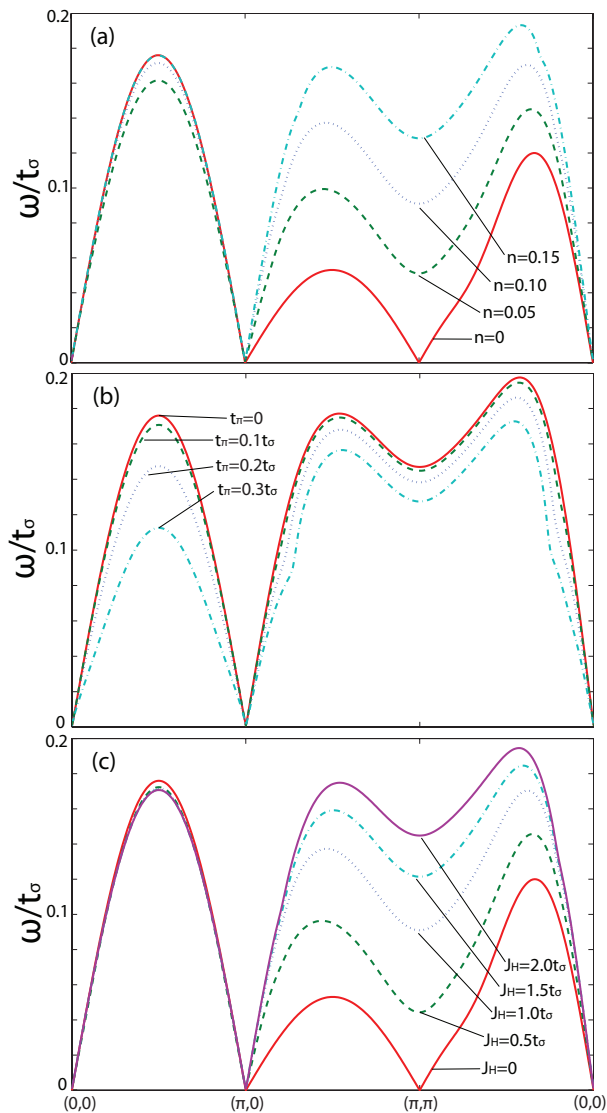


FIG. 3: (Color online) Spin-wave energy ω in the unit of t_σ as a function of the momentum q along the path $(0,0)$ - $(\pi,0)$ - (π,π) - $(0,0)$ in the Brillouin zone containing one Fe atom per unit cell. All the three graphs share the following common parameters: the core spin length $S = 1/2$; the bare exchange constants $J_1 = 0.04t_\sigma$, $J_2 = 0.6J_1$; and the Coulomb repulsion $V = 0$. (a) different filling levels n , $t_\pi = 0.1t_\sigma$, $J_H = 1.0t_\sigma$; (b) different hopping anisotropies, $n = 0.1$, $J_H = 2.0t_\sigma$; (c) different Hund's couplings J_H , $n = 0.1$, $t_\pi = 0.1t_\sigma$.

trated with $J_2 = 0.6J_1$.

When $n = 0$, corresponding to an empty itinerant band, our model reduces to an isotropic J_1 - J_2 Heisenberg model. In this case, the linear spin-wave energies are zero at both $(\pi, 0)$ and (π, π) . At finite electron densities $n < \bar{n}$, we observe that the spin-wave energy at (π, π) is pushed to higher values as n increases. This indicates a stabilization of the stripe antiferromagnetism over the competing Néel order. It is also noted that the spin-wave dispersion along the $(0,0)$ - $(\pi,0)$ direction is nearly unaffected because of the small t_π ($t_\pi = 0.1t_\sigma$) used here.

When $n > \bar{n}$, the anisotropy weakens with increasing filling n . This becomes manifest in a decreasing spin-wave energy at (π, π) . As the filling level continues to rise, the spin-wave spectrum becomes unstable, not shown in the graph, suggesting that the system may evolve to a different ground state, possibly to a spin-disordered, superconducting state.

We also calculate the spin-wave spectra for different hopping anisotropies t_π/t_σ , shown in Fig. 3(b), with Hund's coupling $J_H = 2.0t_\sigma$ and filling $n = 0.1$. Fig. 2(b) indicates that complete ferro-orbital order persists for all the t_π 's considered here. As t_π increases, the ferromagnetic double-exchange contribution along the x -direction is enhanced, resulting in a significant mode softening along the $(0,0)$ - $(\pi,0)$ direction. However, since t_σ remains the same, the corrections to the spin-wave dispersion are almost unaffected along the $(\pi,0)$ - (π,π) direction, equivalent to the $(0,0)$ - $(0,\pi)$ direction. Continuing to decrease the hopping anisotropy (increase t_π) reduces the orbital order, eventually destroying it. We find that around $t_\pi/t_\sigma \simeq 1/3$, the spin-wave spectrum becomes unstable signaling a change of ground states. Therefore, in order to achieve the desired spin-wave spectrum, a strong hopping anisotropy is essential in our model.

Finally, Fig. 3(c) shows the spin-wave spectra for different values of the Hund's coupling J_H , which represents the interaction strength between the local moments and the itinerant electrons. The parameters used are the same as above, and $t_\pi = 0.1t_\sigma$, $n = 0.1$. According to Fig. 2(a), we have complete orbital polarization for all the J_H 's used in Fig. 3(c), except for $J_H = 0.5t_\sigma$. As expected, a larger J_H produces stronger corrections to the spin-wave dispersion.

To conclude, we note that all the above calculations are done for $V = 0$. On the mean field level, this particular Coulomb interaction only affects the relative energy difference between the two orbitals, but has no effect within the same orbital. Consequently, as long as the orbital polarization remains perfect, turning on a finite V does not change the spin-wave dispersion. However, when $n > \bar{n}$, with both orbitals being occupied, increasing V may drive the system back to the ferro-orbital ordered state and stabilize the $(\pi, 0)$ stripe antiferromagnetism.

C. Magnetic anisotropy

In Section IV B we saw that the double exchange leads to a dramatic change of the magnetic excitation spectra. In particular, the spin-wave modes at the Néel antiferromagnetic wave vector (π, π) are almost pushed to a maximum consistent with the neutron-scattering data.⁴⁴ Since the orbital ordering leads to a dramatic anisotropy in the electronic structure, the ferromagnetic double-exchange contribution is expected to be much larger along the y -direction along which the ferromagnetic spin chains are formed. To quantify the induced magnetic anisotropy, in this Section, we fit the spin-wave dispersions calculated

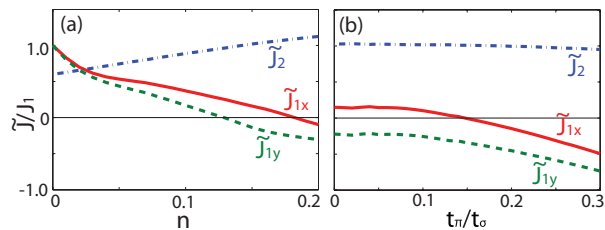


FIG. 4: (Color online) The fitted, effective exchange constants \tilde{J}_{1x} , \tilde{J}_{1y} and \tilde{J}_2 as functions of (a) the filling n , and (b) the hopping anisotropy t_π/t_σ . We use the set of parameters as in Fig. 3(a) and (b), respectively. The effective exchange couplings are expressed in the unit of the bare nearest-neighbor super-exchange J_1 , defined in Eq. (2).

in the presence of both super- and double-exchange to an effective, anisotropic \tilde{J}_{1x} - \tilde{J}_{1y} - \tilde{J}_2 Heisenberg model,

$$\mathcal{H}_{\text{loc}}^{\text{eff}} = \frac{\tilde{J}_{1x}}{S^2} \sum_{\langle i,j \rangle \| \mathbf{x}} \mathbf{S}_i \cdot \mathbf{S}_j + \frac{\tilde{J}_{1y}}{S^2} \sum_{\langle i,j \rangle \| \mathbf{y}} \mathbf{S}_i \cdot \mathbf{S}_j + \frac{\tilde{J}_2}{S^2} \sum_{\langle\langle i,j \rangle\rangle} \mathbf{S}_i \cdot \mathbf{S}_j, \quad (19)$$

where the fitting parameters \tilde{J}_{1x} , \tilde{J}_{1y} and \tilde{J}_2 are the effective exchange constants of nearest neighbors along the x - and y -direction, and next-nearest neighbors, respectively. Please note the different symbols used here to distinguish those in the original Heisenberg model \mathcal{H}_{loc} (2). In the relevant regime $\tilde{J}_{1x} > \tilde{J}_{1y}$, $\tilde{J}_{1y} < 2\tilde{J}_2$, where the $(\pi, 0)$ stripe antiferromagnetism is stable, the linear-spin wave dispersion $\tilde{\omega}(q)$ is determined by $\tilde{\omega}^2(q) = \tilde{A}^2(q) - \tilde{B}^2(q)$ with $\tilde{A}(q) = \tilde{J}_{1x} - \tilde{J}_{1y}(1 - \cos q_y) + 2\tilde{J}_2$ and $\tilde{B}(q) = \tilde{J}_{1x} \cos q_x + 2\tilde{J}_2 \cos q_x \cos q_y$.³⁸

Our fitting results are shown in Fig. 4(a) as functions of the filling level n , with other parameters being the same as in Fig. 3(a). As the number of itinerant electrons increases, both \tilde{J}_{1x} and \tilde{J}_{1y} decrease, the latter faster due to the stronger ferromagnetic double-exchange contribution along the y -direction. However, when $n > \bar{n}$, the electrons start to populate the d_{xz} orbitals causing a faster decrease of \tilde{J}_{1x} . Interestingly, around $n = 0.12$, \tilde{J}_{1y} becomes slightly negative, which completely removes the frustration in the effective spin-only model (Eq. (19)). Such an effective negative exchange coupling along the ferromagnetic direction has been used phenomenologically to rationalize the spectra measured by inelastic neutron scattering.⁴⁴ Remarkably, our calculation shows that the ferromagnetic double-exchange contribution along the y -direction can indeed exceed the bare super-exchange J_1 yielding an effective ferromagnetic exchange \tilde{J}_{1y} .

As a next step, we carry out the fitting process for the spectra with different hopping anisotropies t_π/t_σ [see Fig. 3(b)]. The extracted dependence of the effective exchange constants on t_π/t_σ is shown in Fig. 4(b). As men-

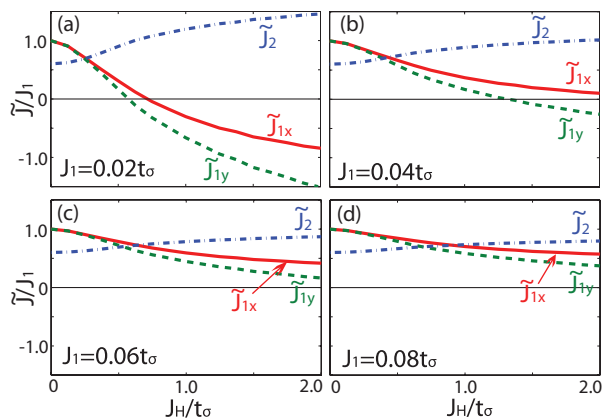


FIG. 5: (Color online) The fitted, effective exchange constants \tilde{J}_{1x} , \tilde{J}_{1y} and \tilde{J}_2 as functions of the Hund's coupling J_H for different bare exchange constants J_1 . (a) $J_1 = 0.02t_\sigma$; (b) $J_1 = 0.04t_\sigma$; (c) $J_1 = 0.06t_\sigma$; (d) $J_1 = 0.08t_\sigma$. In all cases, the ratio of the bare exchange constants is given by $J_2/J_1 = 0.6$ corresponding to the regime of strong frustration.

tioned previously, throughout the plotted region, a complete ferro-orbital order is maintained. Because of the relatively large Hund's coupling of $J_H = 2.0t_\sigma$, for a filling $n = 0.1$, \tilde{J}_{1y} stays negative for all the t_π 's used here. In order for \tilde{J}_{1x} to remain positive, a small t_π/t_σ is required as seen in the graph. In the regime of strong anisotropies, $t_\pi/t_\sigma \lesssim 0.1$, the effective exchange shows almost no dependence on the ratio t_π/t_σ . These results demonstrate that a strong hopping anisotropy is essential in order to induce an unfrustrated $(\pi, 0)$ -antiferromagnetic state.

Finally, in Fig. 5, we analyze the dependence of the effective exchange couplings on the strength of the Hund's coupling J_H . As expected, a large J_H causes a significant correction to the exchange constants. Moreover, as J_H increases, \tilde{J}_{1y} always drops faster relative to \tilde{J}_{1x} . Particularly, we perform the fitting for four different bare nearest-neighbor exchanges J_1 , with Fig. 5(b) corresponding to Fig. 3(c). As shown by the graphs, the larger the bare spin exchanges, the smaller the relative corrections from itinerant bands. In order to achieve the experimentally observed negative \tilde{J}_{1y} within reasonable parameter space, we require $J_1 \lesssim 0.05t_\sigma$. In fact, inelastic neutron scattering⁴⁴ suggests that the exchange constants are of the order of 10 meV, which in our theory leads to an electronic bandwidth and a Hund's coupling J_H both of the order of 1 eV, in agreement with other experimental estimates.²⁶

To conclude this Section, we stress that the degenerate double-exchange model explains the strong magnetic anisotropy observed experimentally.⁴⁴ In a realistic parameter regime, the double-exchange contribution along the ferromagnetic direction can exceed the bare antiferromagnetic super-exchange, J_1 , leading to an effective exchange \tilde{J}_{1y} which is slightly ferromagnetic, consistent with the data. In this regime, the $(\pi, 0)$ antiferromagnetism is unfrustrated. In our model we find that the

$(\pi, 0)$ magnetism is not only stabilized by the anisotropy between the nearest-neighbor exchanges but also by an increase of the effective next-nearest-neighbor coupling \tilde{J}_2 which is found to be larger than in the experiment. Certainly, the inclusion of diagonal hopping amplitudes in our model might lead to reduction of \tilde{J}_2 .

V. DISCUSSION AND CONCLUSION

In summary, we have studied a degenerate double-exchange model for the iron pnictides which explains the dramatic magnetic^{43,44} and electronic⁵¹ anisotropies in these materials. The model consists of local moments which are coupled by antiferromagnetic super-exchanges J_1 and J_2 between nearest- and next-nearest-neighbor spins, respectively, and of itinerant electrons in the bands of the degenerate d_{xz} and d_{yz} orbitals. The electrons are coupled to the local moments by a ferromagnetic Hund's exchange, J_H . The system spontaneously develops ferro-orbital order because of the kinetic energy gained by directing the itinerant electrons along ferromagnetic spin chains which are stabilized by the double-exchange mechanism.

The calculated spin-wave spectra in the presence of both super- and double-exchange are found to be in good agreement with the neutron-scattering data.^{43,44} In particular, we find that the spin-wave dispersion is pushed almost to a local maximum at the competing Néel ordering wave vector as seen in the experiment.⁴⁴ This stabilization of $(\pi, 0)$ -antiferromagnetic order results from the strong anisotropy in the electronic sector which makes the ferromagnetic double-exchange much stronger along the y -direction. Remarkably, in a realistic parameter regime, we find that the ferromagnetic double-exchange can exceed the super-exchange J_1 between the local moments leading to a slightly ferromagnetic exchange \tilde{J}_{1y} along the y -direction in an effective spin-only model. In this regime, the $(\pi, 0)$ antiferromagnetism is unfrustrated.

It is feasible that the parent, undoped materials self-tune the size of the local moments and the carrier density to the point where the $(\pi, 0)$ antiferromagnetism is most stable. In our theory, this is the case for the optimal fill-

ing level $n = \bar{n}$. In fact, the starting Heisenberg model of Eq. (2) is likely to be in the regime of strong frustration, $J_2 \sim 0.5J_1$, leading to a spin disordered ground state in the absence of itinerant electrons. Only through interaction with the ferro-orbital ordered itinerant bands, does the stripe antiferromagnetism emerge. Electron or hole doping the system at $n = \bar{n}$ diminishes the orbital order and thus increases the magnetic frustration, lowering the transition temperature to a spin-ordered state.

The optimal doping levels \bar{n} accessible in our model are certainly too small compared to realistic carrier densities. However, we have seen that the inclusion of an inter-orbital Coulomb repulsion leads to a significant increase of \bar{n} . Therefore, we believe that the careful incorporation of the various interactions between the itinerant electrons⁶¹ as well as diagonal hopping amplitudes would permit accessing higher doping levels and produce realistic Fermi surfaces. However, we point out that because of the electron-electron interactions and the Hund's coupling to the local moments, the hopping amplitudes in the degenerate double-exchange model will be very different from the various sets of tight-binding parameters^{32,60} used to reproduce the desired electron and hole pockets.

We conclude by stressing that the degenerate double-exchange model motivated and studied in this work qualitatively explains many properties of the undoped and slightly doped iron pnictides. The emergent ferro-orbital order breaks the in plane lattice symmetry, thereby driving the orthorhombic lattice distortion. Further, orbital order induces a strong electronic anisotropy which explains why the structural transition is accompanied by dramatic Fermi-surface reconstructions⁵² and transport anomalies.⁵³ Moreover, recent STM experiments⁵¹ have unambiguously demonstrated the spatial anisotropy of the electronic structure below the structural transition temperature. Finally, the orbital ordering produces the strong magnetic anisotropy, essential to explain the experimentally observed magnetic excitation spectra.^{43,44}

Acknowledgments

This work is partially funded by NSF under Grant No. DMR-0940992.

¹ Y. Kamihara, T. Watanabe, M. Hirano, and H. Hosono, *J. Am. Chem. Soc.* **130**, 3296 (2008).
² X. H. Chen, T. Wu, G. Wu, R. H. Liu, H. Chen, and D. F. Fang, *Nature (London)* **453**, 761 (2008).
³ G. F. Chen, Z. Li, D. Wu, G. Li, W. Z. Hu, J. Dong, P. Zheng, J. L. Luo, and N. L. Wang, *Phys. Rev. Lett.* **100**, 247002 (2008).
⁴ Z. A. Ren, G. C. Che, X. L. Dong, J. Yang, W. Lu, W. Yi, X. L. Shen, Z. C. Li, L. L. Sun, F. Zhou, et al., *Europhys. Lett.* **83**, 17002 (2008).
⁵ H. H. Wen, G. Mu, L. Fang, H. Yang, and X. Y. Zhu,

Europhys. Lett. **82**, 17009 (2008).
⁶ M. Rotter, M. Tegel, and D. Johrendt, *Phys. Rev. Lett.* **101**, 107006 (2008).
⁷ S. A. Kivelson and H. Yao, *Nature Materials* **7**, 927 (2008).
⁸ J. Zaanen, *Nature* **457**, 546 (2009).
⁹ S. Tesanovic, *Physics* **2**, 60 (2009).
¹⁰ C. de la Cruz, Q. Huang, J. W. Lynn, W. R. J. Li, J. L. Zarestky, H. A. Mook, G. F. Chen, J. L. Luo, N. L. Wang, and P. Dai, *Nature (London)* **453**, 899 (2008).
¹¹ J. Zhao, Q. Huang, C. de la Cruz, S. Li, J. W. Lynn, Y. Chen, M. A. Green, G. F. Chen, G. Li, Y. Li, et al.,

- Nature Materials **7**, 953 (2008).
- ¹² J. Zhao, Q. Huang, C. de la Cruz, J. W. Lynn, M. D. Lumsden, Z. A. Ren, J. Yang, X. Shen, X. Dong, Z. Zhao, et al., Phys. Rev. B **78**, 132504 (2008).
 - ¹³ S. A. J. Kimber, D. N. Argyriou, F. Yokaichiya, K. Habicht, S. Gerischer, T. Hansen, T. Chatterji, R. Klingeler, C. Hess, G. Behr, et al., Phys. Rev. B **78**, 140503(R) (2008).
 - ¹⁴ A. I. Goldman, D. N. Argyriou, B. Ouladdiaf, T. Chatterji, A. Kreyssig, S. Nandi, N. Ni, S. L. Bud'ko, P. C. Canfield, and R. J. McQueeney, Phys. Rev. B **78**, 100506(R) (2008).
 - ¹⁵ J. Zhao, W. Ratcliff, J. W. Lynn, G. F. Chen, J. L. Luo, N. L. Wang, J. Hu, and P. Dai, Phys. Rev. B **78**, 140504(R) (2008).
 - ¹⁶ Q. Huang, Y. Qiu, W. Bao, M. A. Green, J. W. Lynn, Y. C. Gasparovic, T. Wu, G. Wu, and X. H. Chen, Phys. Rev. Lett. **101**, 257003 (2008).
 - ¹⁷ S. D. Wilson, Z. Yamani, C. R. Rotundu, B. Freelon, E. Bourret-Courchesne, and R. J. Birgeneau, Phys. Rev. B **79**, 184519 (2009).
 - ¹⁸ Y. Chen, J. W. Lynn, J. Li, G. Li, G. F. Chen, J. L. Luo, N. L. Wang, P. Dai, C. dela Cruz, and H. A. Mook, Phys. Rev. B **78**, 064515 (2008).
 - ¹⁹ J. Dong, H. J. Zhang, G. Xu, Z. Li, G. Li, W. Z. Hu, D. Wu, G. F. Chen, X. Dai, J. L. Luo, et al., Europhys. Lett. **83**, 27006 (2008).
 - ²⁰ J. Wu, P. Phillips, and A. H. C. Neto, Phys. Rev. Lett. **101**, 126401 (2008).
 - ²¹ K. Haule, J. H. Shim, and G. Kotliar, Phys. Rev. Lett. **100**, 226402 (2008).
 - ²² L. Craco, M. S. Laad, S. Leoni, and H. Rosner, Physical Review B **78**, 134511 (2008).
 - ²³ K. Nakamura, R. Arita, and M. Imada, J. Phys. Soc. Japan **77**, 093711 (2008).
 - ²⁴ V. Vildosola, L. Pourovskii, R. Arita, S. Biermann, and A. Georges, Physical Review B **78**, 064518 (2008).
 - ²⁵ V. I. Anisimov, D. M. Korotin, S. V. Streltsov, A. V. Kozhevnikov, J. Kunes, A. O. Shorikov, and M. A. Korotin, JETP Lett. **88**, 729 (2008).
 - ²⁶ W. L. Yang, A. P. Sorini, C.-C. Chen, B. Moritz, W.-S. Lee, F. Vernay, P. Olalde-Velasco, J. D. Denlinger, B. Delley, J.-H. Chu, et al., Physical Review B **80**, 014508 (2009).
 - ²⁷ Q. Si and E. Abrahams, Phys. Rev. Lett. **101**, 076401 (2008).
 - ²⁸ C. Fang, H. Yao, W.-F. Tsai, J. P. Hu, and S. A. Kivelson, Phys. Rev. B **77**, 224509 (2008).
 - ²⁹ C. Xu, M. Mueller, and S. Sachdev, Phys. Rev. B **78**, 020501(R) (2008).
 - ³⁰ I. I. Mazin, D. J. Singh, M. D. Johannes, and M. H. Du, Phys. Rev. Lett. **101**, 057003 (2008).
 - ³¹ K. Kuroki, S. Onari, R. Arita, H. Usui, Y. Tanaka, H. Kontani, and H. Aoki, Phys. Rev. Lett. **101**, 087004 (2008).
 - ³² S. Raghu, X.-L. Qi, C.-X. Liu, D. J. Scalapino, and S.-C. Zhang, Phys. Rev. B **77**, 220503(R) (2008).
 - ³³ A. V. Chubukov, D. V. Efremov, and I. Eremin, Phys. Rev. B **78**, 134512 (2008).
 - ³⁴ V. Cvetkovic and Z. Tesanovic, Europhys. Lett. **85**, 37002 (2009).
 - ³⁵ F. Wang, H. Zhai, Y. Ran, A. Vishwanath, and D.-H. Lee, Phys. Rev. Lett. **102**, 047005 (2009).
 - ³⁶ P. M. R. Brydon and C. Timm, Phys. Rev. B **80**, 174401 (2009).
 - ³⁷ T. Yildirim, Phys. Rev. Lett. **101**, 057010 (2008).
 - ³⁸ F. Krüger, S. Kumar, J. Zaanen, and J. van den Brink, Phys. Rev. B **79**, 054504 (2009).
 - ³⁹ H. C. Jiang, F. Krüger, J. E. Moore, D. N. Sheng, J. Zaanen, and Z. Y. Weng, Phys. Rev. B **79**, 174409 (2009).
 - ⁴⁰ G. S. Uhrig, M. Holt, J. Oitmaa, O. P. Sushkov, and R. R. P. Singh, Phys. Rev. B **79**, 092416 (2009).
 - ⁴¹ R. Applegate, J. Oitmaa, and R. R. P. Singh, Phys. Rev. B **81**, 024505 (2010).
 - ⁴² B. Schmidt, M. Siahatgar, and P. Thalmeier, cond-mat/arXiv:0911.5664.
 - ⁴³ J. Zhao, D.-X. Yao, S. Li, T. Hong, Y. Chen, S. Chang, W. R. II, J. W. Lynn, H. A. Mook, G. F. Chen, et al., Phys. Rev. Lett. **101**, 167203 (2008).
 - ⁴⁴ J. Zhao, D. T. Adroja, D.-X. Yao, R. Bewley, S. Li, X. F. Wang, G. Wu, X. H. Chen, J. Hu, and P. Dai, Nature Physics **5**, 555 (2009).
 - ⁴⁵ P. Chandra and B. Doucot, Phys. Rev. B **38**, 9335 (1988).
 - ⁴⁶ C. L. Henley, Phys. Rev. Lett. **62**, 2056 (1989).
 - ⁴⁷ P. Chandra, P. Coleman, and A. I. Larkin, Phys. Rev. Lett. **64**, 88 (1990).
 - ⁴⁸ W. Lv, J. Wu, and P. Phillips, Phys. Rev. B **80**, 224506 (2009).
 - ⁴⁹ C.-C. Lee, W.-G. Yin, and W. Ku, Phys. Rev. Lett. **103**, 267001 (2009).
 - ⁵⁰ W.-C. Lee and C. Wu, Phys. Rev. Lett. **103**, 176101 (2009).
 - ⁵¹ T.-M. Chuang, M. P. Allan, J. Lee, Y. Xie, N. Ni, S. L. Budko, G. S. Boebinger, P. C. Canfield, and J. C. Davis, Science **327**, 181 (2010).
 - ⁵² T. Shimojima, K. Ishizaka, Y. Ishida, N. Katayama, K. Ohgushi, T. Kiss, M. Okawa, T. Togashi, X.-Y. Wang, C.-T. Chen, et al., Phys. Rev. Lett. **104**, 057002 (2010).
 - ⁵³ M. A. McGuire, A. D. Christianson, A. S. Sefat, B. C. Sales, M. D. Lumsden, R. Jin, E. A. Payzant, D. Mandrus, Y. Luan, V. Keppens, et al., Phys. Rev. B **78**, 094517 (2008).
 - ⁵⁴ A. Akrap, J. J. Tu, L. J. Li, G. H. Cao, Z. A. Xu, and C. C. Homes, Phys. Rev. B **80**, 180502(R) (2009).
 - ⁵⁵ S.-P. Kou, T. Li, and Z.-Y. Weng, Europhys. Lett. **88**, 17010 (2009).
 - ⁵⁶ J. Dai, Q. Si, J.-X. Zhu, and E. Abrahams, Proc. Nat. Acad. Sci. **106**, 4118 (2009).
 - ⁵⁷ J. van den Brink and D. Khomskii, Phys. Rev. Lett. **82**, 1016 (1999).
 - ⁵⁸ J. van den Brink, G. Khaliullin, and D. Khomskii, Phys. Rev. Lett. **83**, 5118 (1999).
 - ⁵⁹ J. van den Brink and D. Khomskii, Phys. Rev. B **63**, 140416(R) (2001).
 - ⁶⁰ A. Moreo, M. Daghofer, J. A. Riera, and E. Dagotto, Phys. Rev. B **79**, 134502 (2009).
 - ⁶¹ A. M. Oleś, Phys. Rev. B **28**, 327 (1983).
 - ⁶² E. L. Nagaev, Phys. Rev. B **58**, 827 (1998).
 - ⁶³ D. I. Golosov, Phys. Rev. Lett. **84**, 3974 (2000).
 - ⁶⁴ N. Shannon and A. V. Chubukov, Phys. Rev. B **65**, 104418 (2002).